

Computing the Central Charge of the 3D Ising CFT Using Quantum Finite Elements

Anna-Maria E. Glück,^{a,b,*} George T. Fleming,^{b,c} Richard C. Brower,^d Venkitesh Ayyar,^d Evan K. Owen,^d Timothy G. Raben^e and Chung-I Tan^f

^aHeidelberg University, 69117 Heidelberg, Germany

^bYale University, Sloane Physics Laboratory, New Haven, CT 06511, USA

^cFermi National Accelerator Laboratory, Batavia, IL 60510, USA

^dBoston University, Boston, MA 02215, USA

^eMichigan State University, East Lansing, MI 48824, USA

^fBrown University, Providence, RI 02912, USA

E-mail: anna-maria.glueck@stud.uni-heidelberg.de

The 3D Ising conformal field theory (CFT) describes different physical systems, such as uniaxial magnets or fluids, at their critical points. In absence of an analytical solution for the 3D Ising model, the scaling dimensions and operator product expansion (OPE) coefficients characterizing this CFT must be determined numerically. The currently most-cited values for these quantities have been obtained from the conformal bootstrap, while lattice calculations have so far only produced reliable results for the scaling dimensions involved in calculating the critical exponents. Using Quantum Finite Elements to investigate critical ϕ^4 -theory on $\mathbb{R} \times \mathbb{S}^2$, we show in this work that it is possible to extract scaling dimensions and OPE coefficients of the 3D Ising CFT by fitting the lattice four-point function with expectations from the operator product expansion for the radially quantized CFT and extrapolating to the continuum limit. This way, we have for the first time been able to use Monte Carlo simulations to compute the central charge of the theory.

*The 39th International Symposium on Lattice Field Theory,
8th-13th August, 2022,
Rheinische Friedrich-Wilhelms-Universität Bonn, Bonn, Germany*

*Speaker

1. Introduction

Despite its simplicity, the investigation of the 3D Ising model at criticality is of great relevance as a plethora of phenomena in different areas of physics, from condensed matter to high energy physics, are described by theories in the Ising universality class [1]. Without an analytical solution for the 3D Ising model, the investigation of its critical point has been driven by approximate methods over the last few decades (for an overview, see Ref. [1]). For a long time, the most precise theoretical predictions for the critical exponents of the 3D Ising model were those obtained by applying finite-size scaling arguments to results from Monte Carlo simulations carried out on finite Euclidean lattices using spin-cluster algorithms [1]. In the last decade, however, another method has drastically reduced the error bars: the numerical conformal bootstrap [2, 3]. The bootstrap imposes crossing symmetry on four-point functions and uses the conformal symmetry of the theory describing the critical 3D Ising model - the 3D Ising Conformal Field Theory (CFT) - to identify bounds on the CFT data. Under the hypothesis that the central charge of the 3D Ising CFT should be minimized (c-minimization), the bootstrap achieved extremely precise predictions for scaling dimensions and OPE coefficients of primary operators of this CFT [2–4]. The scaling dimensions for some primaries like σ and ϵ are directly related to the critical exponents for physical quantities in the Ising model [2] that are also well-known from lattice calculations, while the OPE coefficients are extremely hard to compute with usual Monte Carlo methods. However, despite c-minimization being well-motivated, it is an unproven hypothesis, and it is extremely difficult to estimate the systematic error it may introduce to the bootstrap results.

In Refs. [5, 6], a new approach to investigate the 3D Ising CFT was introduced. Adding perturbative counterterms, the so-called Quantum Finite Elements (QFE), to the lattice action and tuning to the critical surface, Brower et al. succeeded at quantizing ϕ^4 -theory on a series of simplicial lattices approximating $\mathbb{R} \times \mathbb{S}^2$ such that the 3D Ising CFT was reached in the continuum limit. After their investigation of the 2-point function of the 0^- -operator σ yielded a value for its scaling dimension that compared favorably with the bootstrap result, the present work is intended as a proof of concept to show that using QFE, it is possible to gain information on the \mathbb{Z}_2 -even sector of the 3D Ising CFT, including the OPE coefficients and the central charge, from lattice calculations of the scalar four-point function on $\mathbb{R} \times \mathbb{S}^2$. The central charge is especially interesting to compute due to both its physical relevance [7, 8] and its role in the bootstrap’s c-minimization hypothesis.

This work is structured as follows: In Sec. 2, we discuss the critical Ising model from the conformal field theory point of view and derive a partial wave expansion for the four-point function in a special antipodal frame on $\mathbb{R} \times \mathbb{S}^2$; Sec. 3 is intended as a reminder of the QFE method, which we employ to carry out lattice calculations of critical ϕ^4 -theory on lattices approaching $\mathbb{R} \times \mathbb{S}^2$; in Sec. 4, we illustrate our data collection and fitting process; finally, we present our results in Sec. 5.

2. The scalar four-point function in the 3D Ising CFT

At its critical temperature $T = T_C$ and in the continuum limit, the 3D Ising model can be described by a conformal field theory, the 3D Ising CFT. CFTs are quantum field theories that are invariant under the conformal group of all angle-preserving space-time transformations [7]. The local operator content of a CFT is spanned by the so-called primary operators, which have special

transformation properties under the conformal group, and their descendants, created by acting on primaries with translation generators. Because operator product expansions (OPEs) are exact for CFTs, the invariant four-point function amplitude g for identical scalar primaries can be written as a series expansion in all primary operators \mathcal{O} [9, 10]:

$$g(u, v) \equiv \frac{\langle \phi(x_1)\phi(x_2)\phi(x_3)\phi(x_4) \rangle}{\langle \phi(x_1)\phi(x_2) \rangle \langle \phi(x_3)\phi(x_4) \rangle} = 1 + \sum_{\mathcal{O}} f_{\phi\phi\mathcal{O}}^2 G_{\mathcal{O}}(\Delta_{\mathcal{O}}; u, v), \quad (1)$$

where $G_{\mathcal{O}}$ are the so-called conformal blocks, functions of the scaling dimension $\Delta_{\mathcal{O}}$ of a given \mathcal{O} and the standard conformally invariant cross ratios u and v . The factors $f_{\mathcal{O}_i\mathcal{O}_j\mathcal{O}_k}$ are called OPE coefficients and can be interpreted as coupling constants in 3-point interactions of primaries. The quantities $\Delta_{\mathcal{O}}$ and $f_{\mathcal{O}_i\mathcal{O}_j\mathcal{O}_k}$ for all primaries fully characterize all n -point functions of a CFT.

The conformal blocks $G_{\mathcal{O}}$ have no known analytic expression in odd dimensions d [9]. However, as a function of the conformal invariants τ and α with $\cosh(\tau) = (1 + \sqrt{v})/\sqrt{u}$ and $\cos(\alpha) = (1 - \sqrt{v})/\sqrt{u}$, they can be expanded in the Gegenbauer polynomials $C_j^{d/2-1}$ [11]

$$G_{\mathcal{O}}(\Delta_{\mathcal{O}}; \tau, \alpha) = \sum_{n \in 2\mathbb{N}_0} e^{-(\Delta_{\mathcal{O}}+n)\tau} \sum_j B_{n,j}(\Delta_{\mathcal{O}}) C_j^{d/2-1}(\cos \alpha). \quad (2)$$

Here, the second sum is carried out over $j \in \{\max(0, l-n), \dots, l+n\}$, where l is the spin of the primary \mathcal{O} , and the $B_{n,j}$ can be calculated recursively as detailed in Ref. [12].

2.1 The antipodal four-point function for the 3D Ising CFT in radial quantization

In our $d = 3$ case, we can now transform from \mathbb{R}^3 to $\mathbb{R} \times \mathbb{S}^2$, defining $t = \log r$:

$$ds_{flat}^2 = r^2 [dt^2 + d\Omega_{d-1}^2] \xrightarrow{\text{Weyl}} ds_{cylinder}^2 = dt^2 + d\Omega_{d-1}^2 = \frac{1}{r^2} ds_{flat}^2. \quad (3)$$

This choice of coordinates is known as radial quantization. Because for a CFT, n -point functions transform as $\langle \phi(x_1)\dots\phi(x_n) \rangle_{flat} = \langle \phi(x_1)\dots\phi(x_n) \rangle_{cylinder} / (r_1^2 \dots r_n^2)$ under this Weyl rescaling, Eq. (1) stays invariant. If we consider a special antipodal frame on $\mathbb{R} \times \mathbb{S}^2$ in which the points $x_i = (t_i, \mathbf{n}_i)$, $i \in \{1, 2, 3, 4\}$ lie pairwise at cylinder-time coordinates $t_1 = t_2$ and $t_3 = t_4$ and the points at the same timeslice are located on opposite sides of the sphere (see Fig. 1a), the time separation $t = |t_1 - t_3|$ and the angle θ with $\cos(\theta) = \mathbf{n}_1 \cdot \mathbf{n}_3$ are mapped to the conformal invariants $\cos(\theta) = \cos(\alpha)$ and $\cosh(t) = \cosh(\tau)$ [6]. Thus, Eq.(2) implies in this antipodal frame:

$$g(t, \theta) = 1 + \sum_{\mathcal{O}} f_{\phi\phi\mathcal{O}}^2 \sum_{n \in 2\mathbb{N}_0} e^{-(\Delta_{\mathcal{O}}+n)t} \sum_j B_{n,j}(\Delta_{\mathcal{O}}) P_j(\cos \theta). \quad (4)$$

The normalization of the coefficients $B_{n,j}(\Delta_{\mathcal{O}})$ in $d = 3$ dimensions is fixed to $B_{0,j}(\Delta_{\mathcal{O}}) = 4^{\Delta_{\mathcal{O}}} \frac{\Gamma(\Delta_{\mathcal{O}})}{\Gamma(\Delta_{\mathcal{O}}/2)^2} \delta_{j,l}$ where $(\cdot)_l$ is the Pochhammer symbol. To calculate the $B_{n,j}(\Delta_{\mathcal{O}})$ for arbitrary (n, j) , we used the Mathematica Notebook provided with Ref. [12]. Because we are considering identical operators in a frame with symmetry under $\theta \rightarrow -\theta$ at each timeslice, only \mathcal{O} with even spin and parity will have non-zero contributions to Eq. (4).

It is convenient to rewrite $g(t, \theta)$ into a form that highlights that it is a partial wave expansion:

$$g(t, \theta) = \sum_{j \in 2\mathbb{N}_0} c_j(t) P_j(\cos \theta). \quad (5)$$

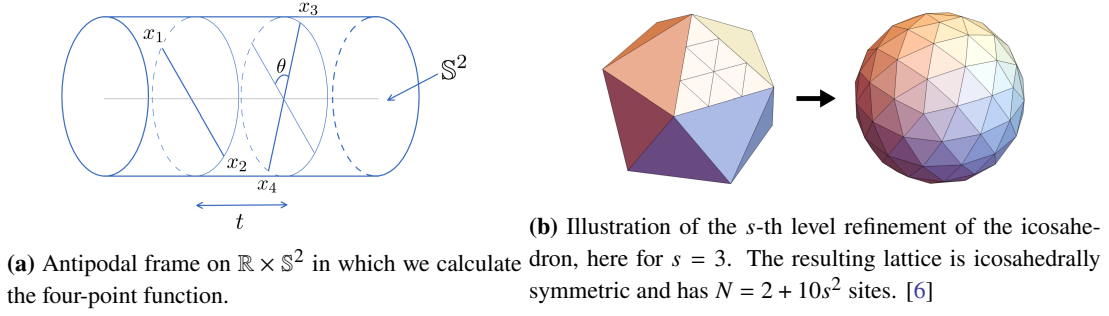


Figure 1: Illustration of the antipodal frame on $\mathbb{R} \times \mathbb{S}^2$ and the lattice construction.

The coefficients $c_j(t)$ can be read off Eq. (4) and are made up of infinitely many terms involving all primaries with even spin l and even parity, with the leading contribution from each spin- l operator O to c_j proportional to $e^{-(\Delta_O + |j-l|)t}$. For example, the leading terms contributing to c_2 are:

$$\begin{aligned}
c_2(t) = & f_{\phi\phi T}^2 B_{0,2}(\Delta_T) e^{-\Delta_T t} + f_{\phi\phi\epsilon}^2 e^{-(\Delta_\epsilon + 2)t} \left(B_{2,2}(\Delta_\epsilon) + B_{4,2}(\Delta_\epsilon) e^{-2t} + \dots \right) \\
& + f_{\phi\phi T'}^2 e^{-\Delta_{T'} t} \left(B_{0,2}(\Delta_{T'}) + B_{2,2}(\Delta_{T'}) e^{-2t} + B_{4,2}(\Delta_{T'}) e^{-4t} + \dots \right) \\
& + f_{\phi\phi\epsilon'}^2 e^{-(\Delta_{\epsilon'} + 2)t} \left(B_{2,2}(\Delta_{\epsilon'}) + B_{4,2}(\Delta_{\epsilon'}) e^{-2t} + \dots \right) + \dots
\end{aligned} \tag{6}$$

Here, we have explicitly included the four even-spin and -parity operators of the 3D Ising CFT with the lowest leading exponentials $\Delta_O + |j-l|$ for $j = 0, 2$, which are ϵ, ϵ' (0^+) and T, T' (2^+).

The OPE coefficient appearing in the contribution of the energy-momentum tensor T to the four-point function is related to the central charge C_T of the 3D Ising CFT via [10]

$$f_{\phi\phi T}^2 = \frac{\Delta_\phi^2 \Delta_T^2}{16C_T}. \tag{7}$$

3. Critical ϕ^4 -theory on $\mathbb{R} \times \mathbb{S}^2$ with Quantum Finite Elements

In Refs. [5, 6], Brower et al. developed Quantum Finite Elements (QFE) as a quantum extension of the classical finite element method. Using QFE, they were able to carry out Monte Carlo calculations of ϕ^4 -theory, a theory in the Ising universality class, on a series of simplicial lattices approaching $\mathbb{R} \times \mathbb{S}^2$, tuned to the critical surface such that the 3D Ising CFT was recovered in the continuum limit [6]. In the following, we will recapitulate the key points of QFE. The reader is referred to Refs. [5, 6] for details.

To approximate \mathbb{S}^2 with constant radius R , a series of simplicial lattices is constructed by subdividing the edges into s pieces and projecting the resulting vertices onto the sphere (see Fig. 1b). The lattice action is then obtained by discretizing the classical ϕ^4 -action using the discrete exterior calculus implementation of the finite element method on this simplicial complex and its Voronoi dual, as well as introducing perturbative counterterms (second line in Eq. (8)), the so-called Quantum Finite Elements, that cancel the UV defects introduced by the position-dependent finite

element weights l_{xy}/l_{xy}^* and $\sqrt{g_x}$ in the classical lattice action [6]:

$$S = \frac{1}{2} \left[\sum_{\langle x,y \rangle} \frac{l_{xy}^*}{l_{xy}} (\phi_{t,x} - \phi_{t,y})^2 + \frac{a^2}{4R^2} \sqrt{g_x} \phi_{t,x}^2 + \sqrt{g_x} \left[\frac{a^2}{a_t^2} (\phi_{t,x} - \phi_{t+1,x})^2 + m_0^2 \phi_{t,x}^2 + \lambda_0 \phi_{t,x}^4 \right] \right] - \sum_{t,x} \sqrt{g_x} \left[6\lambda_0 \delta G_x - 24\lambda_0^2 \delta G_x^{(3)} \right] \phi_{t,x}^2. \quad (8)$$

Here, a is the average lattice spacing on the sphere, related to the radius via $a^2/R^2 = \frac{8\pi}{\sqrt{3}N}$, and a_t is the lattice spacing along \mathbb{R} . While the bare speed of light a/a_t is set to one, it is renormalized by interactions. The terms δG_x and $\delta G_x^{(3)}$ appearing in the counterterms are calculated numerically from the free lattice propagator $G_{t,x;t',y}$ via

$$\delta G_x \equiv G_{t,x;t,x} - \frac{1}{N} \sum_{x'=1}^N \sqrt{g_{x'}} G_{t,x';t,x'}; \quad \delta G_x^{(3)} \equiv \sum_{t',y} \sqrt{g_y} \left[G_{t,x;t',y}^3 - \frac{1}{N} \sum_{x'=1}^N \sqrt{g_{x'}} G_{t,x';t',y}^3 \right]. \quad (9)$$

The dimensionless parameters in this action were tuned to the critical surface by studying the Binder cumulant for fixed $\lambda_0 = 0.2$, finding $m_0^2 = -\mu_0^2 = -0.27018(4)$ as the critical mass [6]. In the following, we will fix the bare parameters to these values for our analysis.

4. Measuring and fitting the lattice four-point function data

In the present work, we used the QFE method to measure the amplitude $g(t, \theta)$ (Eq. (1)) in the antipodal frame introduced in Sec. 2 for the fields ϕ of ϕ^4 -theory tuned to the critical surface. We then projected this amplitude onto Legendre polynomials to access its expansion coefficients $c_j(t)$ (see Eq. (5)). From fits to these coefficients at different lattice spacings, we subsequently extracted values for the scaling dimensions and OPE coefficients for primary operators of the 3D Ising CFT. Finally, we performed first extrapolations of these lattice results to the continuum limit $a/R \rightarrow 0$.

The simulations were carried out with the Tamayo-Brower cluster algorithm [13] combined with Metropolis and overrelaxation at lattice refinements $s \in \{24, 28, 32, 36, 40, 44, 48, 56, 64\}$, with $O(8000)$ independent simulations for $s = 24$, $O(1600)$ for $s = 28-48$ and $O(800)$ for $s = 56, 64$. In the flat direction of our manifold, we used $N_t = 16s$ timesteps and periodic boundary conditions. Fig. 2a shows the results for the first ten non-zero coefficients calculated at $s = 64$ up to maximal times t_{max}^j chosen such that the relative statistical error of the effective mass never exceeds 50%.¹

We note that the properties of the four-point function discussed in Sec. 2 and especially the OPE (Eq. (4)) are only true for CFTs, while our finite lattice spacing breaks conformal symmetry. However, because this symmetry is restored for $a/R \rightarrow 0$, we still fit the $c_j(t)$ with the expectation from the OPE using fit functions like Eq. (6) and assume that for small a/R , the effect of symmetry breaking can be absorbed into a/R -dependent corrections of the parameters $\Delta_{\mathcal{O}}$ and $f_{\phi\phi\mathcal{O}}$ that vanish as $a/R \rightarrow 0$. To be able to insert t given in units of a_t into the continuum fit functions, we have to include the factor $a_t/R = a/(Rc_R)$ with the renormalized speed of light $c_R = a/a_t$ in

¹Compared to the data showed at the conference, the statistics for $s = 32-48$ have been doubled, $s = 28$ has been added and the criterion for the maximal timeslices has been chosen more conservatively and consistently among the different s .

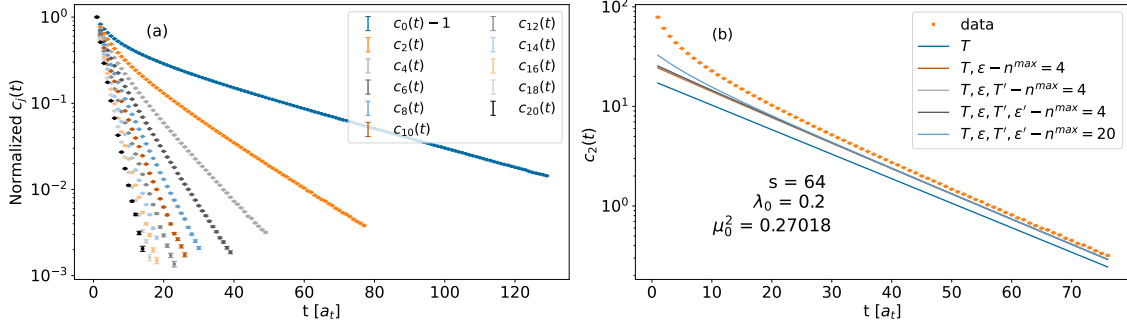


Figure 2: Lattice data for $s = 64$. **(a)** Partial wave expansion coefficients $c_j(t)$ for $j \in 2\mathbb{N}$, $j \leq 20$, normalized by $c_j(1)$. The error bars show the statistical error from averaging over independent Monte Carlo runs. **(b)** Lattice data for $c_2(t)$ compared to continuum predictions based on Eq. (6), including different primaries \mathcal{O} and n_O^{max} . The theoretical curves are not fits but use values determined by the (lightcone) bootstrap [2–4] for $\Delta_{\mathcal{O}}$ and $f_{\phi\phi\mathcal{O}}$. As we compare lattice data with the continuum theory, we do not expect perfect agreement.

the exponents, where $c_R = 0.996$ as determined in Ref. [6]. Moreover, because of our periodic boundary conditions, we have to add $e^{-\Delta_{\mathcal{O}}(N_t-t)a_t/R}$ for each $e^{-\Delta_{\mathcal{O}}t a_t/R}$ in our fit functions for c_j .

In the present work, we focus on extracting CFT data for 0^+ - and 2^+ -operators from fits to c_0 and c_2 . The big advantage of performing fits based on the OPE compared to fitting unconstrained exponentials is that for each operator \mathcal{O} , we only need to introduce two new parameters, $\Delta_{\mathcal{O}}$ and $f_{\phi\phi\mathcal{O}}$, to the fit functions for the $c_j(t)$, which then characterize entire blocks of (in principle) infinitely many exponentials. As these parameters should be the same across all c_j , we perform simultaneous fits to c_0 and c_2 . The leading term in c_0 corresponds to the contribution from the primary ϵ , while the leading term for c_2 comes from the energy-momentum tensor T . Apart from ϵ and T , we include the first subleading operators ϵ' , T' in our fits. Though Fig. 2b shows that their inclusion does not change the fit functions much, their addition increases the model probability calculated according to Ref. [14] and limits the excited state contamination of the fit parameters corresponding to ϵ and T . However, including even more subleading $l = 0$ or $l = 2$ -operators led to fit convergence issues. To minimize truncation errors, we used n up to $n_{\epsilon}^{max} = 20$, $n_{\epsilon'}^{max} = 18$, and $n_{T'}^{max} = 16$, chosen such that the highest exponents for the different operator contributions are of the same order of magnitude. For the energy-momentum tensor, which does not contribute to c_0 , we only included $n_T = 0$ [5]. The resulting truncated OPE prediction for c_2 that we use for fitting is shown as the light blue curve in Fig. 2b, plotted using bootstrap values for the scaling dimensions and OPE coefficients. When compared to our lattice data for $s = 64$, a clear discrepancy can be seen at low t , mainly caused by the truncation of contributions from subleading and higher n to the function, while for larger t this theoretical curve agrees reasonably with our data. Similar observations can be made for c_0 .

For each lattice refinement, we performed simultaneous fits to c_0 and c_2 by least square minimization using the L-BFGS-B optimization algorithm implemented in SciPy [15]. We fixed (t_{max}^0, t_{max}^2) as explained above and carried out fits with all possible combinations of starting times (t_0^{min}, t_2^{min}) . As initial guesses for our fit parameters, we used the bootstrap results [3, 4]. For the OPE coefficients, we used the values for $f_{\sigma\sigma\mathcal{O}}$ because the local field operator ϕ has most overlap

with the 0^- -primary σ , with contributions from other primaries going to zero for $a/R \rightarrow 0$. For the lowest values of s , the T -contribution in our fits was often wrongly attributed to the ϵ' - or T' -terms in the fit function, so we imposed the bounds $\Delta_T \geq 2.5$, $\Delta_{\epsilon'} \geq 3$, and $\Delta_{T'} \geq 3.5$ to prevent this kind of mix-up. To select reasonable starting times (t_0^{min}, t_2^{min}) , we used the framework of model averaging developed in Ref. [14]. After rejecting fits that were not able to constrain all parameters or that converged on the bounds (for fits with reasonable model probability $p(M|D)$, the latter only occurred in a few fits for the $\Delta_{\epsilon'}$ parameter), we renormalized $p(M|D)$ and used all fits with $p(M|D) > 10^{-3}$ in the model averaging for which the determined (t_0^{min}, t_2^{min}) were close to the tuple with maximal $p(M|D)$.

5. Fit Results

Despite our efforts to choose (t_0^{min}, t_2^{min}) optimally, we expect the fit results for the quantities associated with the subleading operators ϵ' and T' to still be significantly influenced by excited states as our fits do not include operators with even higher scaling dimensions or higher spin. Thus, we focus on our results for the leading operators ϵ and T in the following. Fig. 3a-d shows our final, model-averaged fit results for Δ_ϵ , $f_{\phi\phi\epsilon}^2$, Δ_T , and $f_{\phi\phi T}^2$ as functions of a/R compared to the continuum bootstrap values from Refs. [2–4] plotted as blue dotted lines. Note that in the case of Δ_ϵ , the bootstrap value is in agreement with countless Monte Carlo results [1], and for Δ_T the continuum value is fixed to be equal to the dimension of the theory. As we only expect our lattice data to agree with the bootstrap in the continuum limit, the plots also show some fits extrapolating our lattice values to $a/R \rightarrow 0$. Because we have not performed a thorough finite-size scaling analysis [16] yet, we do not know the functional dependence of our results on the lattice spacing. For some first naive extrapolations, we performed linear fits, which can be viewed as the first term in a Taylor series expansion of the true functional dependence. We extrapolated based on all data points (green in Fig. 3) and based on only the data for lattice refinements $s \geq 32$ (orange). The resulting extrapolated values at $a/R = 0$ for the different quantities can be read off the legends in Fig. 3. We might want to exclude $s = 24, 28$ in the extrapolations for two reasons: Firstly, for low s (high a/R), we might be too far from the continuum for the OPE-based fit functions to our data for $c_0(t)$ and $c_2(t)$ to be reasonable. Secondly, the linear approximation of the extrapolation gets worse the higher the values of a/R for which we include data points in the extrapolation fit.

Overall, Fig. 3 shows our lattice results to be close to the bootstrap values, and for the quantities associated with operator ϵ , the lattice data has a clear trend towards these values as $a/R \rightarrow 0$. For the quantities associated with T , the errorbars allow for a broad range of slopes, including constant extrapolations, as T only appears in c_2 , which has significantly fewer timeslices of good data than c_0 (see Fig. 2). Improving on the statistics could reduce these error bars and make the a/R -dependence of the lattice data more apparent.

As the relatively large error bars already make our lattice data for Δ_T consistent with $\Delta_T^{(theory)} = 3$ (see Fig. 3b), also both linear extrapolations yield continuum values that agree with the theory value within 2σ . For Δ_ϵ the naive linear extrapolation using all data points yields a continuum value significantly lower than that obtained by the bootstrap (see Fig. 3a), but when the $s = 24, 28$ lattice values are excluded from the fit, there is agreement within 3σ . For $f_{\phi\phi\epsilon}^2$ (see Fig. 3c), the error bars are small enough that just by looking at the data, we can already conclude that our

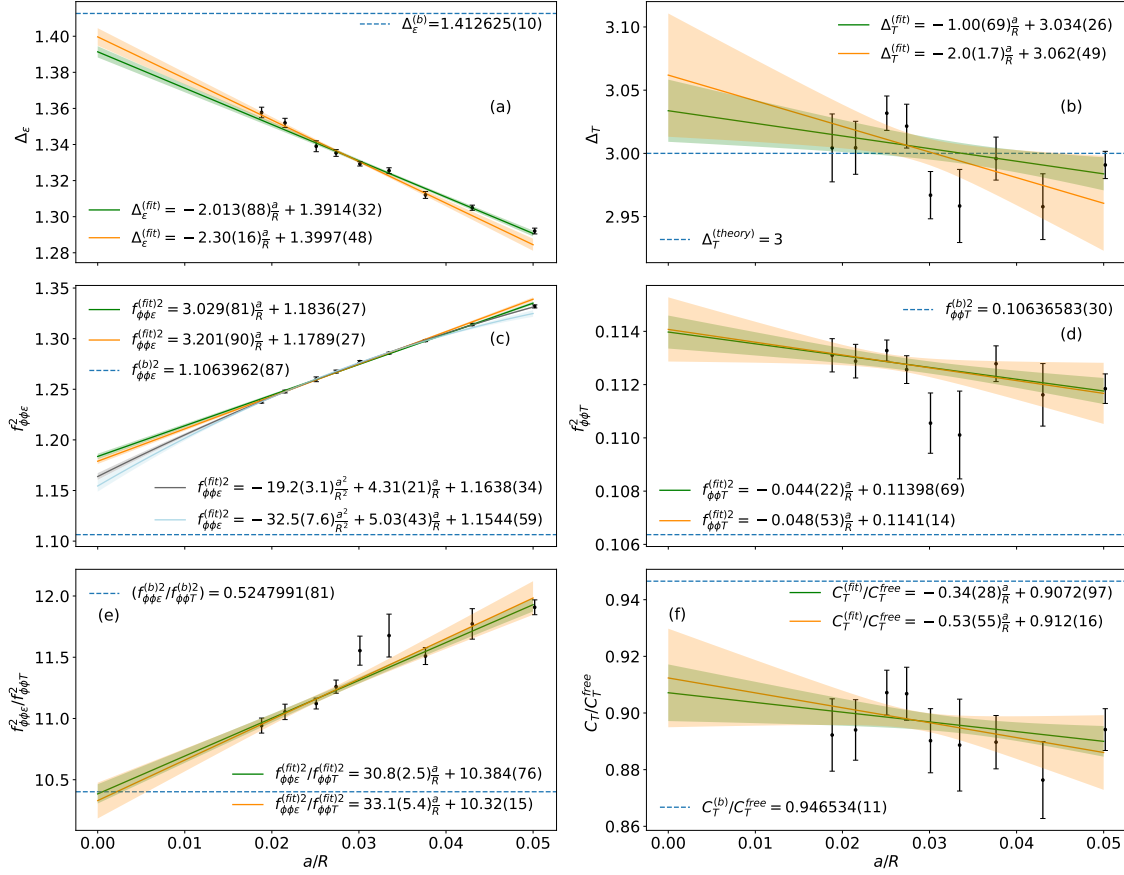


Figure 3: Lattice results for the scaling dimensions and OPE coefficients of the leading operators ϵ and T as well as the central charge a function of the lattice spacing, along with the continuum values obtained from the numerical bootstrap (blue dotted line). First linear fits to extrapolate to $a/R \rightarrow 0$ are shown in green for fits to all data points and in orange for fits to only $s \geq 32$. For $f_{\phi\phi\epsilon}^2$, we also show fits including a quadratic term (grey for fits to all data points, light blue for $s \geq 32$).

lattice results most certainly do not follow a simple linear curve. Therefore, it makes sense that not even the linear fit with $s \geq 32$ yields an extrapolation result consistent with the bootstrap. We tried including a quadratic term as the next order of a possible Taylor expansion, which moved the extrapolation result closer to the bootstrap value. However, the high coefficient in front of the a^2/R^2 -term indicates that the expansion is not convergent for the high values of a/R at which we have data points. This shows that we have to go to lower lattice spacings and, more importantly, use the true a/R -dependence from finite-size scaling as a basis for our extrapolation fits to obtain reliable extrapolation results. In the case of $f_{\phi\phi T}^2$, the linear extrapolations also lead to continuum extrapolations significantly higher than the bootstrap expectation. There even is a slight upwards trend of the lattice results, away from the bootstrap expectation. Such a substantial deviation despite the relatively large statistical errors of the lattice data for $f_{\phi\phi T}^2$ gives us good reason to believe that there also might be considerable systematic errors affecting our calculation, leading to significantly too high values for the OPE coefficients. In the hope of cancelling such systematic errors as well as certain a -dependencies, we show the ratio $f_{\phi\phi\epsilon}^2 / f_{\phi\phi T}^2$ in Fig. 3e. For this ratio, linear extrapolations

Fit	dof	Δ_ϵ	$f_{\phi\phi\epsilon}^2$	Δ_T	$f_{\phi\phi T}^2$	$f_{\phi\phi\epsilon}^2/f_{\phi\phi T}^2$	C_T/C_T^{free}
linear all s	7	12.1	20.8	11.9	7.5	8.2	5.3
linear $s \geq 32$	5	6.3	8.0	9.2	7.3	7.5	3.5

Table 1: χ^2 -values for the linear extrapolation fits.

both including and excluding $s = 24$ and $s = 28$ agree with the bootstrap result within 1σ .

Fig. 3f shows our lattice results for the central charge C_T relative to $C_T^{free} = 3/2$ of the free theory. To calculate C_T at different lattice spacings, we used Eq. (7) with our lattice results for $f_{\phi\phi T}^2$ and Δ_T , as well as $\Delta_\phi = 0.518(2)$, which corresponds to the QFE result from Ref. [6]. Because our values for $f_{\phi\phi T}^2$ are significantly higher than the bootstrap value, our values for the central charge are also lower than the bootstrap prediction. Due to the large error bars and the slight upward trend of C_T/C_T^{free} as $a/R \rightarrow 0$, the linear fit excluding the largest two lattice spacings still extrapolates to a value for the central charge that is consistent with the bootstrap within 2σ . However, possible systematic errors affecting the OPE coefficients and scaling dimensions should also impact our results for the central charge.

6. Discussion and future directions

The goal of the present work was to demonstrate that by fitting the lattice four-point function calculated using the QFE method and subsequently extrapolating the lattice results to $a/R \rightarrow 0$, we can extract scaling dimensions and OPE coefficients as well as the central charge of the 3D Ising CFT. In this proof of concept, we focused on quantities associated with the operator ϵ (0^+) and the energy-momentum tensor T (2^+). For these, we were especially able to obtain the OPE coefficients $f_{\sigma\sigma\epsilon}$ and $f_{\sigma\sigma T}$ as well as the central charge, which has, to the authors' knowledge, not been achieved with Monte Carlo methods before. While for the scaling dimensions and the central charge already linear extrapolations to the continuum are consistent with the bootstrap predictions, this is not the case for the OPE coefficients. To make definite statements about whether or not our continuum extrapolations agree with the bootstrap or even contradict their c-minimization hypothesis, we have to improve our lattice data and extrapolations by using finite-size scaling based extrapolation fit functions, performing simulations at even lower values of a , and improving the statistics of our results. Even more importantly, we have to thoroughly examine and minimize possible systematic errors of QFE and our fitting method.

The big advantage of our lattice calculations compared to the bootstrap, for which the error introduced by the c-minimization hypothesis is hard to estimate, is that both statistical and systematic errors can be systematically improved upon. One possible error source that we are currently investigating is the tuning of our parameters to the critical surface, as even a slight mistuning of μ_0^2 could prohibit us from flowing to the critical theory in the continuum limit. Furthermore, finite-coupling effects could appear because we do not take $\lambda_0 \rightarrow 0$ as we go to the continuum. To investigate and account for these possible errors, we are planning to redo the calculations with $\lambda_0 \rightarrow 0$ as $a/R \rightarrow 0$ and precise fine-tuning of the critical mass for every λ_0 . To get a better understanding of lattice artifacts of the four-point function, we are also currently doing lattice calculations for the free theory on $\mathbb{R} \times \mathbb{S}^2$. Furthermore, we are investigating ways to put the radially

quantized Ising model on a lattice that does not rely on perturbative counterterms. Another source of systematic error goes hand in hand with increasing the statistics of our lattice data: Higher statistics, resulting in a larger range of good timeslices for the c_j , would allow us to include higher-order operators and also higher-spin coefficients c_j to our simultaneous fits, therefore reducing truncation errors and excited state contamination of the coefficients for the leading terms.

After addressing all these issues, the proof of concept in the current work shows that we should be able to obtain low errors - both statistical and systematic - for our lattice results from fitting the c_j . Combined with finite-size scaling based extrapolation fits, this should lead to precise continuum predictions not only for the scaling dimensions and OPE coefficients corresponding to the leading operators but also for subleading and higher- l operators, most of which have only been obtained with the lightcone bootstrap so far. The only obstacle for such improvements is the computational cost. Gathering the data for the current $O(800)$ Monte Carlo runs for $s = 64$ already took $O(6 \times 10^5)$ core hours of computing time running on single cores on the BU shared computing cluster, and the computing time grows $\propto s^3$. Thus, significant improvements in statistics and simulations at higher s would require us to parallelize the code and run on a supercomputer.

7. Acknowledgements

The authors are pleased to acknowledge that the computational work reported on in this paper was performed on the Shared Computing Cluster, which is administered by Boston University's Research Computing Services (www.bu.edu/tech/support/research/). We thank Casey Berger and Andrew D. Gasbarro, whose calculations this work builds upon. This work is supported by the U.S. Department of Energy (DOE) under Award No. DE-SC0019061 for GTF, Award No. DE-SC0015845 for RCB, and Award No. DE-SC0019139 for EKO. AEG acknowledges support from Cusanuswerk Bischöfliche Studienförderung and the Baden-Württemberg Stiftung.

References

- [1] A. Pelissetto and E. Vicari, *Critical phenomena and renormalization group theory*, *Phys. Rept.* **368** (2002) 549–727, [[cond-mat/0012164](https://arxiv.org/abs/cond-mat/0012164)].
- [2] S. El-Showk, M. F. Paulos, D. Poland, S. Rychkov, D. Simmons-Duffin, and A. Vichi, *Solving the 3D Ising Model with the Conformal Bootstrap*, *Phys. Rev. D* **86** (2012) 025022, [[arXiv:1203.6064](https://arxiv.org/abs/1203.6064)].
- [3] S. El-Showk, M. F. Paulos, D. Poland, S. Rychkov, D. Simmons-Duffin, and A. Vichi, *Solving the 3d Ising Model with the Conformal Bootstrap II. c -Minimization and Precise Critical Exponents*, *J. Stat. Phys.* **157** (2014) 869, [[arXiv:1403.4545](https://arxiv.org/abs/1403.4545)].
- [4] D. Simmons-Duffin, *The Lightcone Bootstrap and the Spectrum of the 3d Ising CFT*, *JHEP* **03** (2017) 086, [[arXiv:1612.08471](https://arxiv.org/abs/1612.08471)].
- [5] R. C. Brower, M. Cheng, E. S. Weinberg, G. T. Fleming, A. D. Gasbarro, T. G. Raben, and C.-I. Tan, *Lattice ϕ^4 field theory on Riemann manifolds: Numerical tests for the 2-d Ising CFT on \mathbb{S}^2* , *Phys. Rev. D* **98** (2018), no. 1 014502, [[arXiv:1803.08512](https://arxiv.org/abs/1803.08512)].

- [6] R. C. Brower, G. T. Fleming, A. D. Gasbarro, D. Howarth, T. G. Raben, C.-I. Tan, and E. S. Weinberg, *Radial lattice quantization of 3D ϕ^4 field theory*, *Phys. Rev. D* **104** (2021), no. 9 094502, [[arXiv:2006.15636](#)].
- [7] P. Di Francesco, P. Mathieu, and D. Senechal, *Conformal Field Theory*. Graduate Texts in Contemporary Physics. Springer-Verlag, New York, 1997.
- [8] A. B. Zamolodchikov, *Irreversibility of the Flux of the Renormalization Group in a 2D Field Theory*, *JETP Lett.* **43** (1986) 730–732.
- [9] F. A. Dolan and H. Osborn, *Conformal four point functions and the operator product expansion*, *Nucl. Phys. B* **599** (2001) 459–496, [[hep-th/0011040](#)].
- [10] F. A. Dolan and H. Osborn, *Conformal Partial Waves: Further Mathematical Results*, [arXiv:1108.6194](#).
- [11] M. Hogervorst and S. Rychkov, *Radial Coordinates for Conformal Blocks*, *Phys. Rev. D* **87** (2013) 106004, [[arXiv:1303.1111](#)].
- [12] M. S. Costa, T. Hansen, J. a. Penedones, and E. Trevisani, *Radial expansion for spinning conformal blocks*, *JHEP* **07** (2016) 057, [[arXiv:1603.05552](#)].
- [13] R. C. Brower and P. Tamayo, *Embedded Dynamics for ϕ^4 Theory*, *Phys. Rev. Lett.* **62** (1989) 1087–1090.
- [14] W. I. Jay and E. T. Neil, *Bayesian model averaging for analysis of lattice field theory results*, *Phys. Rev. D* **103** (2021) 114502, [[arXiv:2008.01069](#)].
- [15] R. H. Byrd, P. Lu, J. Nocedal, and C. Zhu, *A limited memory algorithm for bound constrained optimization*, *SIAM Journal on Scientific Computing* **16** (1995), no. 5 1190–1208.
- [16] H. W. J. Blote, E. Luijten, and J. R. Heringa, *Ising universality in three dimensions: a Monte Carlo study*, *J. Phys. A* **28** (1995), no. 22 6289–6313, [[cond-mat/9509016](#)].